Cement & Concrete Composites 31 (2009) 522–534

Contents lists available at ScienceDirect

Cement & Concrete Composites

journal homepage: www.elsevier.com/locate/cemconcomp

Assessment and prediction of RC structure service life by means of durability indicators and physical/chemical models

V. Baroghel-Bouny [a,*], T.Q. Nguyen [a], P. Dangla [b]

[a] Paris Est Univ., Laboratoire Central des Ponts et Chaussées (LCPC), Paris, France
[b] Paris Est Univ., Navier Institute, Champs-sur-Marne, France

ARTICLE INFO

Article history:
Received 2 September 2008
Received in revised form 26 January 2009
Accepted 29 January 2009
Available online 9 February 2009

Keywords:
Chloride
Durability indicator
Moisture
Multi-species
Model
Profile
Specification

ABSTRACT

This paper presents an approach to assess the durability of RC structures, with respect to chloride-induced reinforcement corrosion. The approach is based on durability indicators (DIs). First, performance-based specifications, which involve solely DIs, are proposed for concrete mix-design. In addition, within the framework of service life prediction, a multi-level modelling concept is presented, where DIs are the main input data of the various models. A multi-level physically-based numerical model of chloride ingress has been developed within this framework, and is summarized in the paper. The model offers currently three levels of sophistication in saturated conditions and one level in non-saturated conditions: *level* 1 is a simple chloride diffusion model, *level* 2 is a multi-species model based on *Nernst–Planck* equation, *level* 3 involves transport-chemistry coupling, whereas *level* 4 is a coupled moisture-ion transport model. Examples of application and validation of the model in lab and in field conditions, in particular in the case of wetting–drying cycles, are given in the paper.

1. Introduction

Nowadays, long-term durability of reinforced concrete (RC) structures is a major concern for safety, economical and environmental reasons. Therefore, worldwide efforts are being made to develop lifetime-oriented design concepts and accurate predictive models, in order to ensure a longer lifetime to RC structures at the lowest life-cycle cost and to plan proper maintenance. With the increasing use of complex concrete mixtures, which incorporate supplementary cementing materials (SCM) or recycled products within the framework of sustainable development, a performance-based approach seems particularly relevant for mix-design with respect to durability [1]. Service life (SL) prediction of RC structures encounters at least two major difficulties: the particularly long lifetime required, and the multitude of the possible combinations of solicitations (traffic, mechanical loads, etc.)/aggressions (various types of chemical attacks brought about by either internal or external agents). Therefore, if there is a need for "fine" and long-term predictions, it will be necessary to resort to sophisticated and precise tools. One can refer for example to the comprehensive work performed by Ishida et al. [2,3], who developed a unified computational platform able to predict both material and structural behaviours under coupled actions and various environmental conditions. On the other hand, such tools may appear difficult to use for conventional projects, for example as a result of long computation time, or of the number/nature of input data required.

Hence, a multi-level modelling concept seems to be particularly relevant. It consists in proposing a set of models, covering different levels of sophistication, where the various models are devoted to different issues. Such a concept has been developed within the framework of a general approach based on so-called *durability indicators* (DIs) [4,5], which are key material properties with regard to durability. This approach has been initiated in France in a Working Group (which included many French and also foreign experts) of the *French Association of Civil Engineering* (AFGC) [5]. The purpose of this approach is to design concrete mixtures capable of protecting structures against degradation (e.g. reinforcement corrosion or alkali–silica reaction), for given target lifetime and environmental conditions, thanks to performance-based requirements with respect to the DIs, or conversely to predict the service life of a given new structure at the design stage or the "residual" lifetime of an existing and possibly deteriorated structure (in view of monitoring, diagnosis, maintenance and support to serviceability extension or repair decision). DIs are in this case the main input data of the predictive models. The most advanced models are either deterministic or probabilistic tools that couple well-identified physical and chemical mechanisms. For example with regard to the protection against reinforcement corrosion, in non-saturated conditions, the models include moisture and ion transport, and take into account the microstructural changes induced by the degradation processes

* Corresponding author. Tel.: +33 1 40 43 51 32; fax: +33 1 40 43 54 98.
E-mail address: baroghel@lcpc.fr (V. Baroghel-Bouny).

0958-9465/$ - see front matter © 2009 Elsevier Ltd. All rights reserved.
doi:10.1016/j.cemconcomp.2009.01.009

(e.g. clogging of the pore space by carbonation or crystallisation of salts, increase in the porosity by leaching, or change in the pore structure by formation of *Friedel's* salt C_3A, $CaCl_2$, 10 H_2O). Such models can be used in methods based on inverse analysis, as well as for understanding of mechanisms, accurate and long-term SL prediction, or structural monitoring. The probabilistic feature allows one, in particular, to take into account the uncertainties and the variability of the physical and chemical parameters [5–8]. Within the framework of this approach, simple models are also proposed for engineering purposes (e.g. standard design).

As far as reinforcement corrosion is concerned, chlorides are well-known aggressive species and they are present in various types of environments (marine, coastal, or road submitted to deicing salts). Chlorides can also be present in the original mix ingredients. In saturated conditions, chlorides from the environment penetrate into the covercrete by a coupled diffusion-binding process. This process involves a penetration front, which propagates at finite velocity, depending on the material properties and on the environmental conditions. Therefore, in chloride-contaminated environments, RC structure durability will strongly rely on the location of this front. In non-saturated conditions, advection also takes place. This means that chlorides will be transported with liquid water, under a total (or capillary) pressure gradient, according to the extended *Darcy's* law (see Section 3.4). This induces a higher rate of chloride ingress and of reinforcement corrosion, in particular in the case of wetting–drying cycles, compared to diffusion (i.e. in saturated conditions) [9–11]. Even if some models described in the literature take this advection process into account [10,12–17] (see also the literature reviews presented in [5,18]), most of them do not take into account all of the other physical and chemical mechanisms/processes. In addition, the movements of liquid water (involved in the advection process) and of water vapour are usually not separated, thus inducing errors in the predictions.

In this paper, performance-based specifications are proposed for concrete mix-design, as a function of the environmental conditions and of the target structural SL, where the criteria involve solely DIs. Moreover, within the framework of the described approach, this paper focuses on the understanding of chloride ingress in partially saturated concrete and on SL prediction by means of physically-based models. In particular, the paper deals with a 1-D multi-level numerical model of chloride ingress developed in isothermal conditions. Examples of application and of validation of the model in lab and in field conditions are given, particularly in the case of wetting (by a salt solution) and drying cycles.

2. Durability indicators, associated classes and performance-based specifications

The list of so-called *general DIs,* which are relevant to many degradation processes, has been selected upon the criteria of theoretical relevance in the quantification and the prediction of durability and of easy and reliable assessment by means of validated lab test methods [4,5]. This list includes: (initial) calcium hydroxide (content), porosity (accessible to water), (chloride) ion diffusion coefficient(s), and permeability (to gas and to liquid water). This list may be complemented by so-called *specific indicators* (which are relevant to a given degradation process such as alkali–silica reaction [5] or freeze–thaw damage), or/and by *complementary parameters* (CPs). CPs can be required for example as input data for a predictive model. As a matter of fact, the chloride concentration at the concrete surface (c_s) and the chloride binding isotherm appear as useful CPs with regard to chloride-induced corrosion, more precisely for empirical and physical models of chloride ingress, respectively, (see next sections). Note that (the same) DIs are used for concrete mix-design, as well as for models (as in input data).

A system of classes [5] with respect to the "potential" durability to reinforcement corrosion has been proposed for each general DI. These classes, five levels ranging from very low (VL) to very high (VH) "potential" durability, can be used for mixture comparison. When several DIs have been assessed, the "potential" durability of a RC can be based on an overall weighted rating. Examples are provided in [4].

An illustration of these classes, with regard to the DIs *apparent* gas permeability (at degree of liquid water saturation $S_l = 0$) and *apparent* chloride diffusion coefficient, as well as the range of values covered by these DIs, is provided in Fig. 1 (the VL, L, M, H and VH classes previously defined are reported in the graphs). In this figure, the experimental results, obtained on a large number of concretes ranging from low-grade materials (average 28-day cylinder compressive strength, c.s., around 25 MPa) up to very-high-performance concretes (28-day c.s. > 90 MPa), are plotted *vs.* the average 28-day cylinder c.s. of the materials. Air-entraining admixture (AEA), fly ash (FA), or silica fume (SF) were incorporated in some of the mixtures, and some concretes were prepared with blastfurnace slag cements (CEM III/A, with here 43–64% blastfurnace slag). The gas permeability was measured by the constant head CEMBUREAU apparatus (at inlet gas pressure P_{inlet} = 0.2 MPa) after water curing and oven drying at $T = 105 \pm 5$ °C, according to the AFPC-AFREM procedure [19], whereas the chloride diffusion coefficient was obtained from migration tests under an electrical field in non-steady-state (nss) conditions, on saturated concrete samples, after water curing [20,21]. These experimental data were obtained within the framework of various studies, in particular the AFGC Working Group, the LPC research project "Performance-based and probabilistic durability approach", and the French National Project "BHP 2000" [4,20,22]. In this last project, a broad range of concretes was investigated not only on lab specimens but also on cores extracted from RC structural elements exposed to various natural environments or from actual bridge decks. In the LPC research project, mixtures commonly used in actual bridges in various locations in France were in particular studied.

Fig. 1 clearly illustrates, for a same average 28-day c.s., the efficiency of FA or slag in the reduction of the values of the measured DIs: a higher durability level (class) is reached, compared to plain mixtures with same average 28-day c.s. For example, normal-strength FA-concretes (FA content from 25% to 54% by unit mass of cement) display very low transport properties and a high "potential" durability. The values recorded for these FA-concretes can be very close to that found for high-performance concretes (HPCs). The reduction in the gas permeability and in the chloride diffusion coefficient in saturated conditions, with the increase in the FA content, has been reported in the literature for lab data and also for field data [23–26]. Conversely, the presence of entrained air (2–8% air), which increases the connectivity of the void system, induces a significant increase in the *apparent* gas permeability, in particular for HPCs, which can display a low "potential" durability with respect to the *apparent* gas permeability. However, no systematic effect of the use of AEA is recorded on the *apparent* chloride diffusion coefficient.

For most of the plain mixtures (i.e. without FA, slag and SF) commonly used in actual bridges in various locations in France, a medium "potential" durability was obtained.

More generally Fig. 1 shows that a broad range of transport properties values and different "potential" durabilities can be obtained for a same average 28-day c.s. depending on the mix-composition. This is a clear illustration of the consequences of the new trends of concrete mix-design and of the relevance and usefulness of a performance-based approach for durability assessment of complex mixtures. Mechanical properties are not sufficient to estimate the "potential" durability of a RC and to select appropriate mixtures that meet durability requirements.

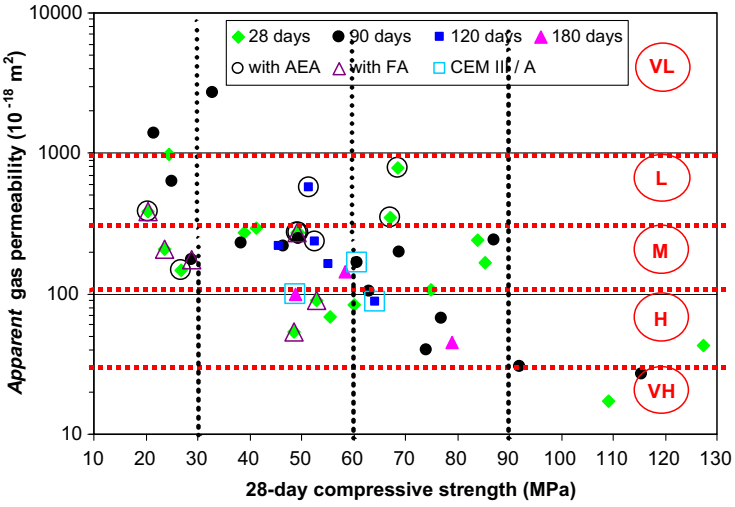

a) *apparent* gas permeability at $S_l = 0$ measured by the CEMBUREAU apparatus (at $P_{inlet} = 0.2$ MPa) after water curing and oven drying at T = 105 ± 5 °C, according to the AFPC-AFREM procedure [19]

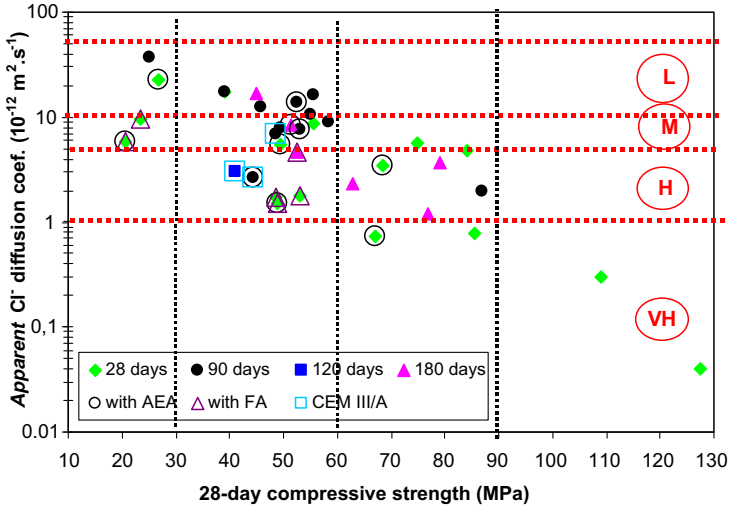

b) *apparent* chloride diffusion coefficient obtained from nss migration tests on saturated concrete samples, after water curing

Fig. 1. Classes of "potential" durability and experimental (average) values of DIs for concrete samples at various ages, *vs*. the average 28-day cylinder compressive strength.

On the basis of these DIs and classes, performance-based specifications have been proposed as a function of the environmental conditions and of the target structural SL, with the purpose of helping designers, structure owners, or contractors, when drafting durability requirements for the selection of concrete mixtures for a given new structure. The criteria have been defined according to experimental data obtained on a broad range of concretes (in particular in the projects previously mentioned) and verified by simulations involving several models (empirical or physical, deterministic or probabilistic) [5].

The specifications proposed for the protection of structures against chloride-induced reinforcement corrosion, when only the *initiation period*, as defined in [27], is regarded (i.e. the limit state is assumed as the depassivation of the first layer of rebars, see Section 6.2), are presented in Table 1, under the assumption that the minimum cover thickness specified in the European regulations is applied ($e = 50$ mm). In Table 1, the porosity accessible to water ϕ has no unit, the *apparent* chloride diffusion coefficient $D_{app(mig)}$, measured by means of a migration test in steady-state (ss) or nss conditions, is given in 10^{-12} m^2 s^{-1}, the *apparent* gas permeability (at $S_l = 0$ and $P_{inlet} = 0.2$ MPa) $K_{app(gas)}$ is expressed in 10^{-18} m^2, and the *intrinsic* liquid water permeability (at $S_l = 1$) k_l is in 10^{-18} m^2. The values indicated in Table 1 refer to concrete samples cured in water for 90 days or less. They are average values, to which the precision of the test methods should be added. For example, the coefficient of variation of the nss chloride migration test is equal to 15% according to [5,21]. As illustrated by Table 1, when both the target SL increases and the environment becomes more aggressive, the number of DIs to check also increases (up to four) and the criteria (threshold values) are more stringent. For example, in the case of immersion in seawater, the specifications refer to the porosity and the chloride diffusion coefficient, whereas in the case of exposure to salts or in tidal zones, permeability is also addressed when a long SL is required. Of course in the practice the suggested criteria can be adapted for specific project conditions depending on the local environment, cover thickness, or economics. The criteria are also likely to evolve when further experience will be obtained. Note that the specifications in Table 1 do not involve the initial (in case of

Table 1
Durability specifications proposed with respect to chloride-induced reinforcement corrosion, according to the environmental conditions and the target service life of the structure (minimum cover thickness = 50 mm).

Environment type → / Target service life ↓	5 Exposure to spraying of marine or deicing salts		6 Immersion in seawater	7 Tidal zone
	5.1 ($c_s \leq 10$ g.L^{-1})	**5.2** ($c_s \geq 100$ g.L^{-1})		
< 30 years	•$\phi < 0.16$	•$\phi < 0.14$	•$\phi < 0.15$	•$\phi < 0.14$
from 30 to 50 years	•$\phi < 0.15$	•$\phi < 0.11$	•$\phi < 0.13$	•$\phi < 0.11$
from 50 to 100 years	•$\phi < 0.14$	•$\phi < 0.11$ •$D_{app(mig)} < 2$ •$k_l < 0.1$	•$\phi < 0.13$ •$D_{app(mig)} < 7$	•$\phi < 0.11$ •$D_{app(mig)} < 3$ •$k_l < 0.1$
from 100 to 120 years	•$\phi < 0.12$ •$D_{app(mig)} < 20$ •$k_l < 0.1$	•$\phi < 0.09$ •$D_{app(mig)} < 1$ •$K_{app(gas)} < 30$ •$k_l < 0.01$	•$\phi < 0.12$ •$D_{app(mig)} < 5$	•$\phi < 0.10$ •$D_{app(mig)} < 2$ •$K_{app(gas)} < 100$ •$k_l < 0.05$
> 120 years	•$\phi < 0.09$ •$D_{app(mig)} < 10$ •$K_{app(gas)} < 30$ •$k_l < 0.01$	•$\phi < 0.09$ •$D_{app(mig)} < 1$ •$K_{app(gas)} < 30$ •$k_l < 0.01$	•$\phi < 0.09$ •$D_{app(mig)} < 1$	•$\phi < 0.09$ •$D_{app(mig)} < 1$ •$K_{app(gas)} < 30$ •$k_l < 0.01$

Colours (or grey levels) refer to the classes previously defined (here, from low to very high "potential" durability).

carbonation or leaching) $Ca(OH)_2$ content. However, this DI is in particular required as input data not only of most of the carbonation models [5], but also of models of chloride ingress (e.g. see Section 3.3).

In France, these specifications, along with those proposed with respect to carbonation-induced reinforcement corrosion [4], have been used in order to select concrete mixtures for new bridges (e.g. Millau bridge). They have also been used to define a set of low-cost and environment-conscious "local" concrete mixtures (including in particular local aggregates and SCM), which meet the 50-to-100-year SL requirements (predefined durability). Such "local" concretes have been defined for each type of environment in France. The resulting pre-characterized concretes will be able to be used in future projects in the considered environment without checking again the DIs.

3. Multi-level model proposed for chloride ingress and service life predictions

The multi-level concept introduced in Section 1 can of course be applied to a single model. This will be illustrated in this section, in the case of the modelling of isothermal chloride ingress into concrete, by the 1-D physically-based numerical model developed at LCPC. This model offers currently three levels of sophistication in saturated conditions and one level in non-saturated conditions. It can therefore be used for engineering purposes as well as for accurate long-term prediction and understanding of complex coupled processes (see next sections). The appropriate level has to be selected in particular according to the purpose of the prediction, the accuracy required, the target structural lifetime, and the availability of the input data.

The system of non-linear equations associated with each level is solved numerically by means of a standard Newton algorithm [28], where the spatial discretization is performed by the finite volume method and where an Euler implicit scheme is used for the approximation of the normal derivatives.

3.1. Level 1 (chloride diffusion model)

This model [29] includes a single species (chlorides) and is based on diffusion (in diluted solution) according to *Fick's* first law. This is a simple model, which requires only a few input data: the DIs porosity accessible to water and *effective* chloride diffusion coefficient (D_{Cl^-}), and the so-called chloride binding isotherm, described here globally by *Freundlich's* non-linear formula (see Eq. (1)):

$$s_{Cl} = \mu c_{Cl^-}^{\gamma} \tag{1}$$

where (c_{Cl^-}) is the chloride concentration of the pore solution (in mol/m^3 of solution) and s_{Cl} the total amount of bound chlorides (in mol/m^3 of material), while μ and γ are the *Freundlich's* isotherm parameters, which vary with the binder composition.

Nevertheless, the "unphysical" variations of D_{Cl^-} *vs.* chloride concentration, observed when using this oversimplified approach (see e.g. [10,30] for mortars), need to be described (fitted) by an empirical law, as those proposed in [31,32]. It can be proven that these "unphysical" variations are the result of neglecting the (electrical) influence of the other ions present in the solution (see [29,33,34]). It is worth noting that, despite this drawback, the single-ion approach is still used, in particular in the methods of assessment of chloride diffusion coefficients by diffusion or migration tests [21], and in a great number of prediction models (see the state-of-the-arts provided in [5,18]). Moreover, such a model can appear as an improvement, compared to the empirical models still often used for predictions in real cases [6] and in model code designs for engineers [7]. Nevertheless, since it is not quite satisfactory from a theoretical point of view, this model will not be discussed further in the present paper.

3.2. Level 2 (multi-species transport model)

This model [34] describes the transport in saturated conditions of some of the various ionic species present in the medium. The ions Cl^-, OH^-, Na^+ and K^+ are addressed here, as usually done by researchers. This model takes into account the electrical interactions between ions. The transport of each ionic species is described by *Nernst–Planck* equation (see Eq. (2)), which includes in the general case three components: diffusion under concentration gradient, movement under chemical activity effects, and migration under the (local) electrical field, which results from the electrical interactions between ions [13,33,35–37]:

$$J_i = -D_i\left[\mathrm{grad}c_i + c_i\mathrm{grad}(\ln\gamma_i) + \frac{z_i F}{RT}c_i\mathrm{grad}\psi\right] \tag{2}$$

where J_i, D_i, c_i, γ_i and z_i are the flux (in mol m^{-2} s^{-1}), the constant *effective* diffusion coefficient of the material (in m^2 s^{-1}), the concentration (in mol/m^3 of solution), the chemical activity coefficient (–) and the valence number (–) associated with each ionic species i, respectively. F is the Faraday constant (9.64846×10^4 C mol^{-1}), R the ideal gas constant (8.3143 J mol^{-1} K^{-1}), T the absolute temperature (in K), and ψ the local electrical potential (in V), which arises in order to maintain electroneutrality in the medium.

Here, the chemical activity coefficients γ_i are set to 1 (as in an ideal solution, i.e. $\{i\} = c_i$, where $\{i\}$ is the activity of ion i), as done by other authors [33], and on the basis of the results presented in [32,34]. As a matter of fact, very similar ionic concentration profiles were found after diffusion tests in usual conditions, with and without including activity effects in the present model [34]. A significant difference was observed only with very high outer chloride concentrations.

The set of mass balance equations for each element either present as an ion or included in a solid compound, reads (see Eq. (3)):

$$\frac{\partial n_i}{\partial t} + \mathrm{div} J_i = 0 \tag{3}$$

where n_i (i = O, H, Cl, Na or K) denotes the total molar content of element i as ionic species or in solid compound. For example, $n_{Cl} = \phi c_{Cl^-} + s_{Cl}$, where s_{Cl} is related to c_{Cl^-} through the chloride binding isotherm.

Various options are proposed in the model for the description and the assessment of the non-linear chloride binding isotherm (see e.g. [11,29,38]). For example, a global description according to *Freundlich's* formula (see Eq. (1)) can be chosen, as often used by researchers [10,30,33,39]. In this case, the *Freundlich's* isotherm parameters will be fitted on experimental data when available, or identified by numerical inverse analysis thanks to the proposed model and to an experimental total chloride concentration (tcc) profile [34,38]. Otherwise, an analytical formula based on the composition of the material [11,38], which includes both physical adsorption onto C–S–H [40] (component s^p_{Cl}) and *Friedel's* salt formation [41,42] (component s^c_{Cl}), can be adopted (see e.g. Eq. (4)). Physical adsorption can be described by *Freundlich's* or *Langmuir's* formula or directly derived from the ionic exchange theory (assuming exchange between chlorides from the pore solution and hydroxyl ions from the C–S–H, see Eq. (4)). *Friedel's* salt formation is assumed here as instantaneous and complete at very low chloride concentrations ($c_{Cl^-} \approx 0$). In this case, the *Friedel's* salt amount formed $s_{Friedel}$ is assumed to be independent of c_{Cl^-} and expressed as a function of the residual equivalent aluminate content of the material at the considered age $N_{(C_3A)eq.}$ (in mol/m^3 of material) (see Eq. (4)):

$$s_{Cl} = s^p_{Cl} + s^c_{Cl} = s^p_{Cl} + 2s_{Friedel} = N_{C-S-H}\frac{\alpha c_{Cl^-}}{c_{OH^-} + \beta c_{Cl^-}} + 2N_{(C_3A)eq.} \tag{4}$$

where N_{C-S-H} denotes the C–S–H content of the material at the considered age (in mol/m^3 of material), and the parameters α and β are assumed to be solely dependent of the C–S–H intrinsic properties and thus independent of the (concrete) mix-composition for given binder type (e.g. CEM I) and age.

In this model, the adsorption of the other ions present in the pore solution is neglected. In order to keep the electroneutrality of the medium, the binding of chlorides is assumed to be balanced by the dissolution of hydroxyls.

The local electroneutrality condition within the medium complements the system of equations (see Eq. (5)):

$$\sum c_i z_i = 0 \tag{5}$$

This equation is the consequence of the general *Poisson's* equation, under some conditions (the other term, which includes ψ, can be neglected at the specimen scale, since the dielectric permittivity of the medium is very low [11,34,37,43,44]). As a matter of fact, same ionic concentration profiles are predicted, when applying the electroneutrality condition or *Poisson's* equation, in the case of diffusion tests in usual conditions [34]. The computations are simplified by selecting the electroneutrality condition. In particular, the dielectric permittivity is no more required.

In addition to the boundary conditions (B.C.), the input data required for this model are the DIs ϕ and D_i, along with the chloride binding isotherm and *initial* chemical composition of the pore solution. These initial conditions (I.C.) can be assessed by means of the analytical method described in [34], which requires the mix-composition, the chemical composition of the cement and an analytical hydration model (e.g. the model proposed in [45]). D_i (with $i \neq Cl^-$) is drawn from D_{Cl^-} (which can be assessed for example by the methods proposed in [5,34,20,21], in particular from ss or nss migration tests) and from Eq. (6):

$$\frac{D_i}{D^o_i} = \frac{D_{Cl^-}}{D^o_{Cl^-}} (= \tau \cdot \phi) \tag{6}$$

where $D^o_{Cl^-}$ and D^o_i are the diffusion coefficients in an infinitely diluted solution, and τ is the tortuosity of the material (–).

3.3. Level 3 (advanced physical and chemical model)

This multi-species model involves transport-chemistry coupling. It is based on the physical principle of ionic mass conservation and on the chemical equilibrium between a solution and the various solid compounds in contact with it. With regard to chloride binding, physical adsorption onto C–S–H (as described in Section 3.2) and *Friedel's* salt formation by chemical reactions (dissolution/precipitation mechanism, see Table 2) are addressed separately. Thus, the model includes, in addition to the equations used in *level* 2, those associated with the dissolution/precipitation equilibriums along with the species involved in these equations [29,46]. Therefore, it requires at least six ions (Ca^{2+}, $Al(OH)^-_4$, Cl^-, OH^-, Na^+ and K^+) and 3 solid compounds (*Friedel's* salt, $Ca(OH)_2$ and aluminates).

For each reaction (see Table 2), chemical equilibrium is satisfied unless the solid compound has totally disappeared. For example, in the case of reaction (a), equilibrium state is characterized by Eq. (7):

$$\{Ca^{2+}\}\{OH^-\}^2 = K_P \quad \text{if } s_{Ca(OH)_2} \neq 0 \tag{7}$$

where K_P and $s_{Ca(OH)_2}$ denote, respectively, the solubility product and the content of calcium hydroxide.

When $Ca(OH)_2$ is completely dissolved, $\{Ca^{2+}\}\{OH^-\}^2$ can be lower than K_P. Therefore, in the general case, Eq. (8) has to be verified:

Table 2
Friedel's salt formation – examples of chemical reactions.

Reactions			$-\log K$
(a)	$Ca(OH)_2 \leftrightarrow Ca^{2+} + 2OH^-$	$K_P = \{Ca^{2+}\}\{OH^-\}^2$	5.05
(b)	$3CaO \cdot Al_2O_3 + 6H_2O \leftrightarrow 3Ca^{2+} + 4OH^- + 2Al(OH)^-_4$	$K_C = \{Ca^{2+}\}^3\{OH^-\}^4\{Al(OH)^-_4\}^2$	22.5
(c)	$3CaO \cdot CaCl_2 \cdot Al_2O_3 \cdot 10H_2O \leftrightarrow 4Ca^{2+} + 4OH^- + 2Al(OH)^-_4 + 2Cl^-$	$K_F = \{Ca^{2+}\}^4\{OH^-\}^4Al(OH)^-_4{}^2\{Cl^-\}^2$	29.1
(d)	$2H_2O \leftrightarrow H_3O^+ + OH^-$	$K_W = \{H_3O^+\}\{OH^-\}$	14

$$\{Ca^{2+}\}\{OH^-\}^2 \begin{cases} = K_P & \text{if } s_{Ca(OH)_2} > 0 \\ < K_P & \text{if } s_{Ca(OH)_2} = 0 \end{cases} \quad (8)$$

The instantaneous dissolution/precipitation process can thus be described by the following condition (see Eq. (9)):

$$\begin{cases} s_{Ca(OH)_2} \geq 0 \\ K_P \geq \{Ca^{2+}\}\{OH^-\}^2 \\ s_{Ca(OH)_2}\left[K_P - \{Ca^{2+}\}\{OH^-\}^2\right] = 0 \end{cases} \quad (9)$$

Such a condition induces a discontinuous $s_{Ca(OH)_2}$ profile. An appropriate change in the variables allows both the ionic activities and the solid contents to appear in the same equations, as detailed in [29,46]. For each reaction, a condition such as Eq. (9) has to be verified at each node of the mesh.

Moreover, the model accounts for the microstructural changes induced by *Friedel's* salt precipitation or $Ca(OH)_2$ dissolution. Hence, with regard to the transport equations, the same type as used in *level* 2 is adopted (see Section 3.2), but here D_i and ϕ are variable. The modified *effective* diffusion coefficients are deduced from the modified porosity provided by the model, thanks to an empirical formula derived from that proposed by Bentz et al. in [47] for hardened cement pastes and based on the capillary porosity (see Eq. (10)):

$$\phi = \phi^{ini} + \sum v_i \Delta s_i \quad \text{and} \quad D_i = D_i^{ini} \frac{\phi}{\phi^{ini}} \left(\frac{\phi^{ini} - 0.18}{\phi - 0.18}\right) \quad (10)$$

where ϕ^{ini} and D_i^{ini} denote, respectively, the initial porosity accessible to water and the initial *effective* diffusion coefficient associated with ion i, while s_i is the amount (in mol/m^3 of material) and v_i the molar volume (in m^3 mol^{-1}) of solid compound i.

At each step, the mass balance equations, the electroneutrality condition and the dissolution/precipitation equilibrium relationships constitute the whole system of equations. Transport equations and chemical equilibrium relationships are solved simultaneously [11]. The computational time is hence significantly reduced, compared to sequential resolution. At each step, the values of D_i are re-evaluated.

Level 3 allows one to take accurately into account the "chemical effect" associated with binding (linked to the chemical composition of the cement matrix), in addition to the "physical barrier effect", within the framework of mix-design optimization to reach a given "potential" durability. Moreover, *level* 3 can allow accurate pH predictions, since the various equations that involve hydroxyl ions are taken into account in the model. Nevertheless, this model requires as input data the initial amount of each ionic and solid species addressed, which can be difficult to assess experimentally.

3.4. Level 4 (coupled moisture-ion transport model)

This is the multi-species model (see *level* 2) extended to non-saturated conditions. The contribution of advection (movement of ions with that of liquid water) to the overall ion transport has to be taken into account in this case (see Eq. (11)):

$$\begin{cases} w_\alpha = v_l c_\alpha + J_\alpha \quad (\alpha = w \text{ or } i, \text{ for liquid water or ions, respectively}) \\ \text{or} \\ w_\alpha = v_g c_\alpha + J_\alpha \quad (\alpha = a \text{ or } v, \text{ for dry air or water vapour, respectively}) \end{cases} \quad (11)$$

where w_α denotes the total molar flux (in mol m^{-2} s^{-1}) of phase α and c_α is the molar concentration of α, with the condition $\sum \upsilon_\alpha c_\alpha = 1$ when $\alpha = w$ or i, for liquid water or ions, respectively, where υ_α is the molar volume of phase α in solution (e.g. υ_w = 18.0 cm^3 mol^{-1} and $v_{Na^+} = 1.5$ cm^3 mol^{-1}).

This means that the model combines the ion transport according to *Nernst–Planck* equation (see Eq. (2), but here D_i are a function of S_l) with the Darcian movement of the liquid phase l (mixture of water and ions) and of the gas phase g (mixture of water vapour and dry air) (see Eq. (12)), and with the relative Fickian diffusion of water vapour and dry air with respect to the gas mixture (see Eq. (13)) [48,49]. v_l and v_g are thus calculated by Eq. (12), and J_α (with $\alpha = a$ or v, for dry air or water vapour, respectively) is calculated by Eq. (13):

$$v_\alpha = -\frac{k_\alpha}{\eta_\alpha} k_{r\alpha}(S_l) \text{grad } p_\alpha \quad (\alpha = l \text{ or } g, \text{for liquid or gas phase, respectively}) \quad (12)$$

where k_α is the intrinsic permeability of the material to phase α, independent of S_l (in m^2), whereas v_α, p_α, η_α and $k_{r\alpha}(S_l)$ denote the *Darcy's* filtration velocity (in m s^{-1}), the pressure (in Pa), the dynamic viscosity (in Pa s) and the relative permeability associated with phase α, respectively,

$$J_\alpha = -\frac{\rho_g}{M_\alpha} f(\phi, S_l) D_{v0} \text{grad}\left(\frac{\rho_\alpha}{\rho_g}\right) \quad (\alpha = a \text{ or } v, \text{for dry air or water vapour, respectively}) \quad (13)$$

where J_α, M_α and ρ_α are the molar flux (in mol m^{-2} s^{-1}), the molar mass (in kg mol^{-1}) and the mass density (in kg m^{-3}) of constituent α, respectively. D_{v0} is the free (out of the porous medium) water vapour diffusion coefficient in the air ($D_{v0} = 2.47 \times 10^{-5}$ m^2 s^{-1} between $T = 20$ and 25 °C), while $f(\phi, S_l)$ is the so-called resistance factor, which accounts for both the tortuosity effects and the reduction of space offered to gas diffusion in a partially saturated porous medium, compared to free diffusion in the air.

Note that the intrinsic permeabilities of the material to gas and to liquid can be different in the model, in order to account for the findings reported in [49,50] (significant different experimental values were found for k_g and k_l, for some mixtures).

Once the diffusive flux J_i of all ions is known, the diffusive molar flux of liquid water J_w (in mol m^{-2} s^{-1}) is computed by using Eq. (14):

$$M_w J_w + \sum_{i \neq w} M_i J_i = 0 \quad (14)$$

where M_w and M_i are the molar masses (in kg mol^{-1}) of water and ion i, respectively.

Finally, the mass balance equations for moisture ($w + v$), dry air (a) and ions i read (see Eq. (15)):

$$\begin{cases} \frac{\partial}{\partial t}\left(\phi S_l c_w + \phi(1 - S_l)\frac{\rho_v}{M_v}\right) = -\text{div}(w_w + w_v) \\ \frac{\partial}{\partial t}\left(\phi(1 - S_l)\frac{\rho_a}{M_a}\right) = -\text{div}(w_a) \\ \frac{\partial}{\partial t}\left(\phi S_l c_i + s_i\right) = -\text{div}(w_i) \end{cases} \quad (15)$$

The ions effect on the liquid-vapour water equilibrium (water–ions coupling) is taken into account by including the chemical activity of liquid water in the solution (a_w) into the chemical potential formula (where a_w is expressed *vs.* the ionic activity coefficients γ_i, according to the formula proposed by Lin and Lee [51]). This results in the extended *Kelvin's* law (see Eq. (16)):

$$p_c = -\frac{\rho_w}{M_w} \text{RT}(\ln h - \ln a_w) \quad (16)$$

where h is the relative humidity (–), ranging in this equation from 0 to 1.

It turned out that including the capillary pressure curve equation $p_c = p_c(S_l)$ of a chloride-free material in Eq. (16) matched with very good agreement the experimental data obtained with the same material with various NaCl concentrations [10,52]. It was thus concluded that the capillary pressure curve is an intrinsic

feature of the (pore structure) of the material and that only the curve of the chloride-free material (derived from the experimental water vapour sorption isotherm [53]) is required as input data for the model. This simplifies significantly the modelling.

As previously described, the model accounts for transport property variations *vs.* S_l. Analytical laws are used here, in order to express such variations and implement them easily in the model. Formulas for $k_{r\alpha}(S_l)$ and $f(\phi,S_l)$ are proposed in [48–50]. The same type of semi-empirical formula as proposed in [54] for masonry materials is adopted here for D_i variations *vs.* S_l (see Eq. (17)):

$$D_i(S_l)/D_i(S_l=1)=S_l^{\lambda} \quad (17)$$

where λ is the saturation exponent.

Calibration of this formula with the various mortar data obtained by impedance spectroscopy and provided in [10] (assuming that the same curve is valid whatever the cementitious material, similarly as k_{rl} [49]) yielded $\lambda = 6$.

With regard to chloride binding, same descriptions (analytical formulas) as proposed in *level* 2 can be used.

Possible crystallization of salts and dissolution/precipitation reactions are not taken into account in *level* 4.

4. Comparison between the multi-species transport model (*level* 2) and the advanced physical and chemical model (*level* 3)

A water-cured sample of normal-strength concrete BO (CEM I 52.5, W/C = 0.49, and average 28-day c.s. = 50.0 MPa) has been exposed in lab to a salt solution (30 g L^{-1} NaCl + NaOH 0.1 M, and thus pH = 13) for 90 days, after vacuum saturation. The material was 90-day old at the beginning of the test. The total and free chloride concentration profiles have been measured by means of dry-grinding and chemical analysis [20]. More precisely, the total (resp. free) chloride concentration has been determined by means of nitric acid (resp. water) extraction and potentiometric titration, according to the AFPC-AFREM procedure [55,56]. The raw free chloride concentration data then obtained have been corrected, as suggested by Otsuki et al. [57] (see also [20]).

The profiles were also predicted by the level-2 model (multi-species transport model with four ions + analytical binding isotherm) and the level-3 model (advanced physical and chemical model with six ions and three solid compounds). As far as possible, the same input data and descriptions were used in both models (e.g. $\phi = 0.12$, $D_{Cl^-} = 1.2\ 10^{-12}$ m^2 s^{-1} assessed by migration tests [20], and initial conditions $c_{Cl^-} = 0, c_{OH^-} = 360, c_{Na^+} = 100$ and $c_{K^+} = 260$ mol m^{-3}, which yield pH = 13.6, assessed by the method described in [34]). The same physical adsorption law (derived from the ionic exchange theory) was adopted for s_{Cl}^{p} (see Eq. (4)) and calibrated with published data obtained by the equilibrium method [38,46]. With regard to *Friedel's* salt formation, in the level-3 model s_{Cl}^{c} is provided by solving the equations associated with the dissolution/precipitation equilibriums (see Section 3.3 and [29,46]), whereas in *level* 2 the simplified analytical description used in Eq. (4) is adopted. The initial composition of the solid matrix (required for application of the level-3 model) is provided by an analytical hydration model [45].

As illustrated in Fig. 2a, the main difference recorded is a higher tcc, from the assumed *Friedel's* salt precipitation front in the level-2 model, up to the actual precipitation front (tcc ≈ 50–80 mol/m^3 of material) provided by the level-3 model. Within this range, level-2 results seem to diverge from both level-3 results and experimental data. Note that in the models the reaction kinetics are neglected; this induces sharp dissolution and precipitation fronts (see Fig. 2a, Section 3.3 and also [11,29]). Therefore, the main difference lays in the simplified description adopted in the level-2 model for *Friedel's* salt formation. Note that *level* 2 is a "conservative" simplification: the tcc predicted in this case is higher compared to *level* 3. Moreover, no difference is observed between level-2 and level-3 results with regard to the c_{Cl^-} profiles and good agreement is observed with experimental data (see Fig. 2b), thus validating the two models in lab conditions (first stage of validation).

A small peak is observed at the surface when applying the level-3 model (see Fig. 2a), as a result of a local porosity increase induced by $Ca(OH)_2$ dissolution (OH^- and Ca^{2+} leaching). Microstructural changes have thus only a slight effect in the present test conditions (only a slight leaching takes place). In these conditions, *level* 2 can be quite sufficient. On the other hand, it will be necessary to use the level-3 model in the cases (e.g. exposure to seawater or to low pH solutions) where microstructural changes can significantly affect the transport process, or in environments where a great number of (aggressive) species are present (and various chemical reactions may occur).

5. Analysis of the effect of wetting–drying cycles on chloride transport by means of the coupled moisture-ion transport model (*level* 4)

5.1. Comparison with lab data from the literature

The effect of wetting (by a salt solution) and drying cycles on the tcc profile can be illustrated by Fig. 3. This figure describes the case, reported by Hong and Hooton in [58], of initially-saturated concrete samples (W/binder = 0.40, 25% slag, 8% SF and 28-

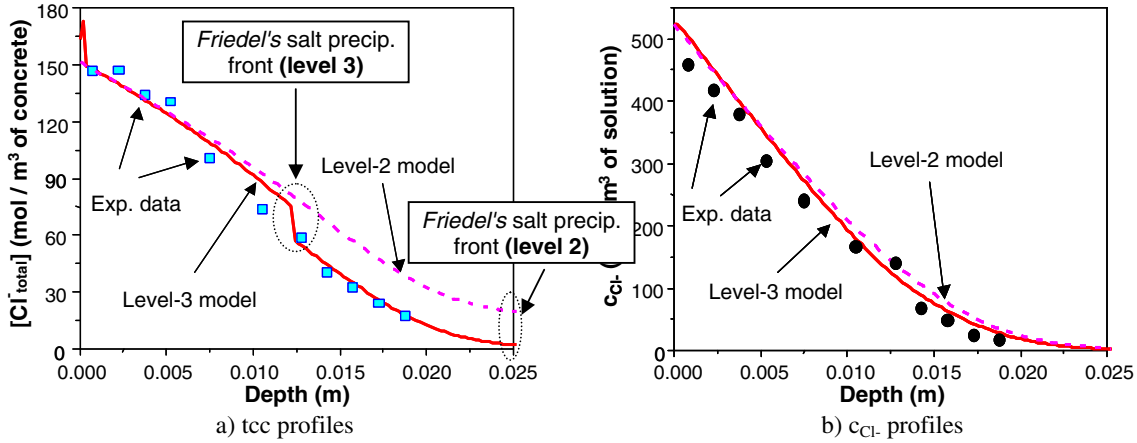

Fig. 2. Tcc and c_{Cl^-} profiles for a concrete sample BO, after 90-day exposure to 30 g L^{-1} NaCl + NaOH 0.1 M in lab. Measurements [20] and numerical simulations performed by the multi-species transport model (*level* 2) and the advanced physical and chemical model (*level* 3).

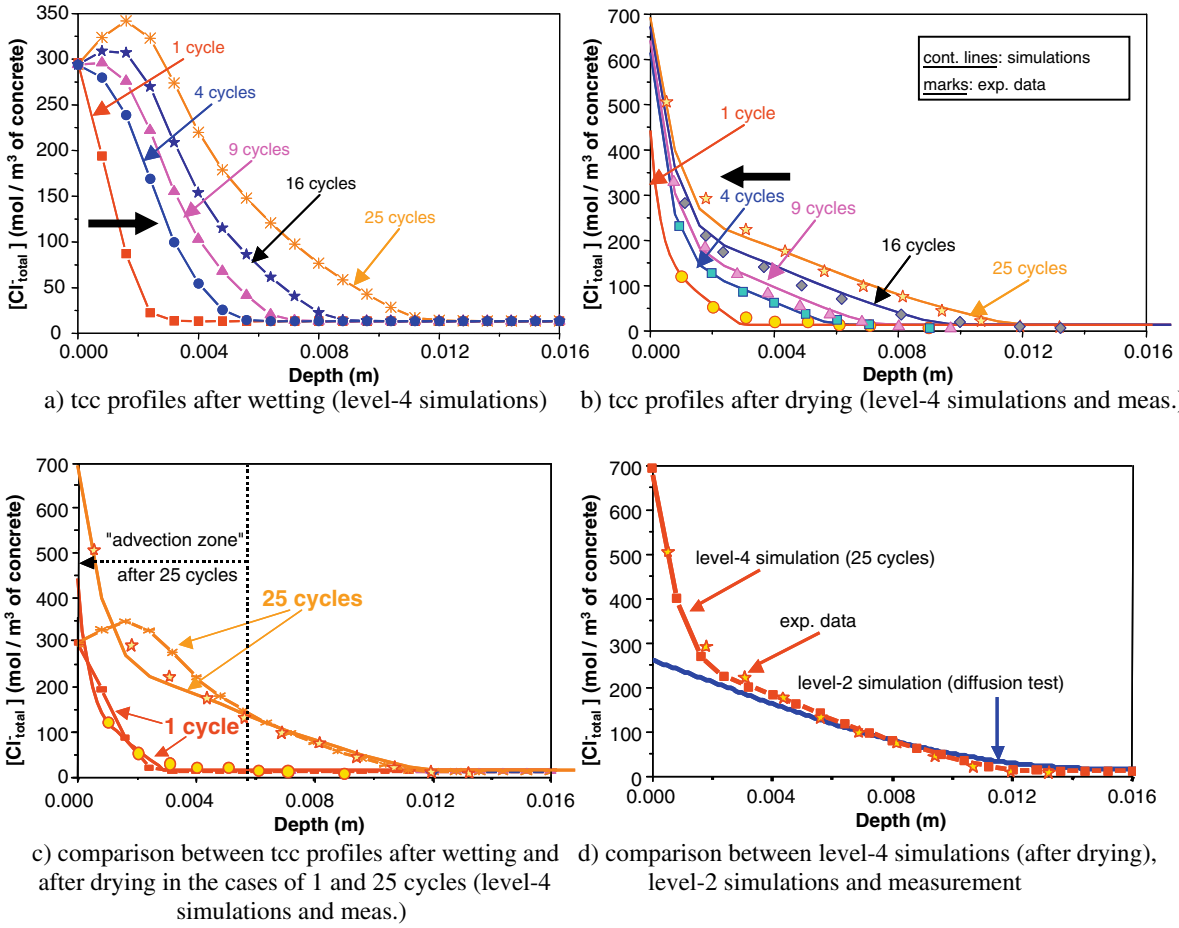

a) tcc profiles after wetting (level-4 simulations)

b) tcc profiles after drying (level-4 simulations and meas.)

c) comparison between tcc profiles after wetting and after drying in the cases of 1 and 25 cycles (level-4 simulations and meas.)

d) comparison between level-4 simulations (after drying), level-2 simulations and measurement

Fig. 3. Effect of wetting–drying cycles on the tcc profiles for a concrete sample in lab (total exposure time: 75 days). Measurements [58] and numerical simulations by the multi-species transport model (*level* 2) and the coupled moisture-ion transport model (*level* 4).

day sealed curing) submitted in lab to 25 cycles (1 cycle = 6-h wetting by 1-M NaCl solution + 66-h drying at $h = 50\%$, at $T = 23$ °C) for a total exposure time of 75 days. The 25 cycles have been simulated by the coupled moisture-ion transport model (*level* 4) by using the porosity, permeabilities (e.g. $k_l = 3.6\ 10^{-21}$ m^2, assessed by inverse analysis) and capillary pressure curve provided in [48,49,53] for concrete BO (see Section 4). D_{Cl^-} ($= 1.02 \times 10^{-12}$ m^2 s^{-1}) has been assessed by inverse analysis (as explained in [34]) from the experimental tcc profile provided by Hong and Hooton, after 120-day exposure to the salt solution in saturated conditions (diffusion test [58]). The numerical tcc profiles after drying (see Fig. 3) have been compared to the experimental data reported in [58] and also to the numerical profile provided by the multi-species transport model in saturated conditions (*level* 2) for the case of a diffusion test (exposure to 1-M NaCl solution for 75 days).

Very good agreement is pointed out in Fig. 3b between level-4 simulations and experimental data. This highlights the validation of the level-4 model in lab conditions (first stage of validation) and confirms, in particular, the relevance of the assumptions made in the modelling.

Fig. 3 points out the difference, within the sample zone affected by the wetting–drying cycles (so-called "advection zone"), between the profiles obtained (by simulation) after wetting (see Fig. 3a) and the profiles obtained (both by simulation and measurement) after drying (see Fig. 3b). This difference is clearly exhibited, in the cases of 1 and 25 cycles, in Fig. 3c. It can be attributed to the different B.C. and prominent transport process between the wetting and drying phases. As a matter of fact, during the wetting phases, as part of the bulk liquid phase, chlorides move inwards mainly by advection in the surface zone. When the inner c_{Cl^-} is higher than the outer one, chlorides tend also to leach out, by outward diffusion. As a result, a peak may appear on the tcc profile (see Fig. 3a). In the course of drying, a significant amount of chlorides from the advection zone moves back with liquid water by advection to the evaporation front. The location of the evaporation front depends on the material and on the experimental conditions. The evaporation front is very close to the surface zone in this example, as a result of the presence of a continuous liquid phase within the whole sample thickness, which allows moisture transport mainly through the liquid phase (according to Eq. (12)) during drying. This results from the considered drying conditions ($h_{min} = 50\%$) and the low permeability of the material (as explained in [48,50]). After cycles, the tcc in the surface zone is higher than the B.C. associated with wetting (as a result of chloride accumulation at the evaporation front) and increases as a function of time (as a result of chloride supply at each wetting phase) (see Fig. 3b).

The difference recorded between the results provided by the level-2 ($S_l = 1$) and level-4 (cycles) models (see Fig. 3d) points out that the cycles, and in particular the drying process, have induced in the advection zone and more precisely in the surface zone a tcc increase, which cannot be predicted by a model developed in saturated conditions. These points out the major contribution of the advective process to the overall ion transport and thus the importance of k_l in the model.

Fig. 4a displays the S_l profiles computed by the level-4 model after various numbers of cycles ($S_l = 1$ at the initial state). Different S_l profiles are here also recorded after wetting and after drying (beneath the wetting front). There is consistence between the

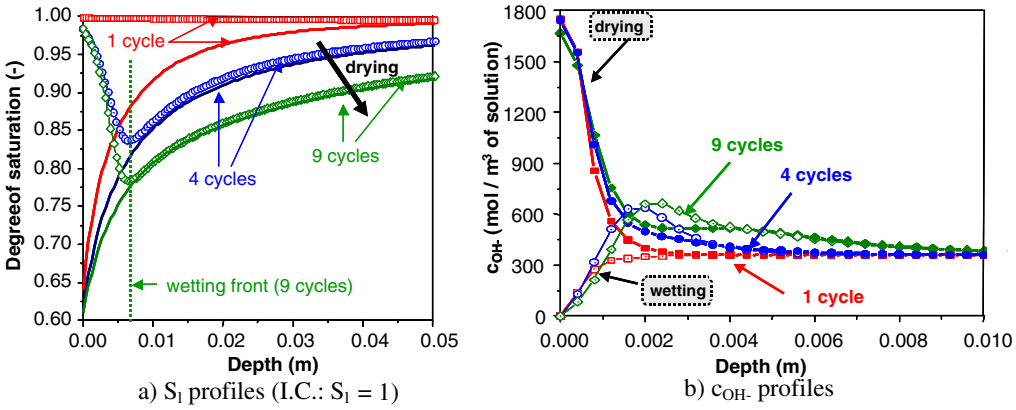

Fig. 4. Effect of wetting–drying cycles for a concrete sample in lab (total exposure time: 75 days). Numerical simulations by the coupled moisture-ion transport model (*level* 4).

wetting fronts deduced from the chloride concentration and S_l profiles. After a few cycles, the moisture state is changed in the whole sample thickness, but the S_l value is not low enough to hinder chloride diffusion in the core of the sample.

Fig. 4b displays c_{OH^-} profiles computed by the level-4 model. During the wetting phases, hydroxyl ions tend to diffuse outward (as a result of lower outer c_{OH^-}). After cycles, a peak appears in the c_{OH^-} profile obtained after wetting, which may result from hydroxyl diffusion and advective flux in opposite directions. Note that after drying, c_{OH^-} is very high in the surface zone, as a result of S_l decrease. This indicates a very low physically bound chloride amount s^p_{Cl} (according to Eq. (4)).

The sample zone affected by the wetting–drying cycles in this example can thus be clearly experimentally and theoretically identified through these various results.

5.2. Effect of varying the exposure conditions on the tcc profile

More generally, the exposure conditions have a significant effect on the tcc profile: any modification of these conditions, even with a same exposure time, induces a noticeable change. This is illustrated in Fig. 5, which displays the numerical simulations performed by the level-4 model in the case of a BO sample submitted, for a total exposure time of 50 days, to various combinations of wetting (by 0.5-M NaCl solution or water) and drying (at h = 75%) cycles.

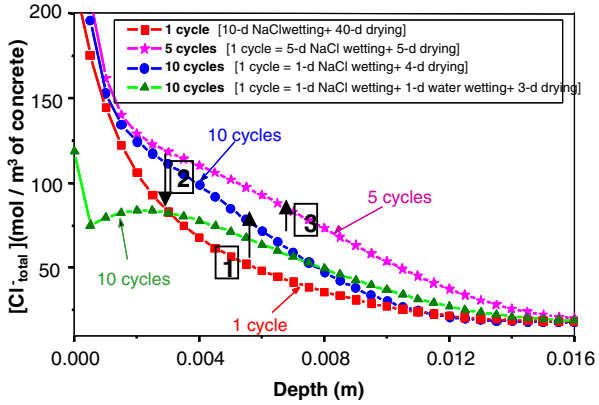

Fig. 5. Effect of exposure conditions (with a same exposure time: 50 days) on the tcc profile for a sample of concrete BO. Simulations performed by the coupled moisture-ion transport model (*level* 4).

As illustrated by the comparison (1) between 1 cycle (10-d NaCl wetting + 40-d drying) and 10 cycles (where 1 cycle = 1-d NaCl wetting + 4-d drying), increasing the cycle number, with the same durations of both the NaCl-exposure period and the drying period, induces an increase in the tcc within a large thickness of the sample. In addition, the effect of 1-day wetting by water induces a redistribution of the tcc from the surface zone and within a large thickness, as illustrated by the comparison (2) between 10 cycles where 1 cycle = 1-d NaCl wetting + 4-d drying, and 10 cycles where 1 cycle = 1-d NaCl wetting + 1-d water wetting + 3-d drying. Note that such an effect is often recorded, as a result of rain, in coastal areas or in marine sites during low tide. Moreover, a longer NaCl exposure period (along with a slightly longer drying period), even in the case of a smaller number of cycles, increases the tcc (see the comparison (3) between 5 cycles, where 1 cycle = 5-d NaCl wetting + 5-d drying, and 10 cycles, where 1 cycle = 1-d NaCl wetting + 4-d drying).

5.3. Experimental results in field conditions

In field conditions, in particular in tidal zones, combinations of the various effects previously described take place, such as increase as a function of time in the cycles number, and increase in the cumulative time of exposure to seawater.

Fig. 6 shows the tcc profiles measured in RC structural elements from the "BHP 2000" Project [22] after various exposure times for two HPCs mixed with the same CEM I 52.5, silica fume and aggregates: M75SF (W/C = 0.38, SF/C = 0.06 and average 28-day c.s. = 85.5 MPa) and M120SF (W/C = 0.26, SF/C = 0.12 and average 28-day c.s. = 127.5 MPa), in a marine environment (tidal zone in La Rochelle, France). These field data have been obtained by chemical analysis, as previously described. The average carbonation depth x_c, measured by phenolphthalein spray test after 10 years, is also reported in Fig. 6: a negligible carbonation has been recorded.

Both the tcc and the free chloride concentration measured in the surface zone after drying were higher than the B.C. associated with total submersion in seawater. In addition, Fig. 6 highlights that the tcc in the surface zone increases as a function of time, at least for a given period of time. In addition to the accumulation phenomenon (which results from wetting–drying cycles) described in Section 5.1, microstructural changes induced by chemical reactions and c_{Cl^-} increase as a result of *Friedel's* salt dissolution after total $Ca(OH)_2$ dissolution (lower $c_{Ca^{2+}}$ and c_{OH^-} of the seawater with pH ≈ 8.8, compared to the pore solution) [29,46] can contribute to explain these observations in the present case. More generally, same findings as predicted by the simulations performed

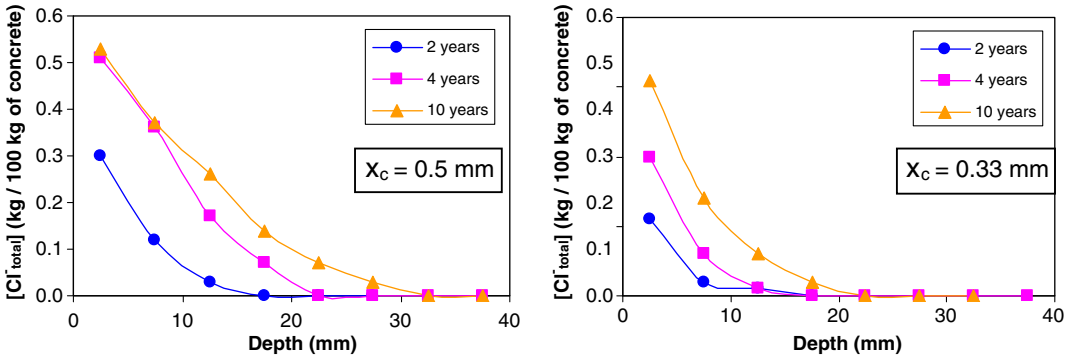

a) concrete M75SF b) concrete M120SF

Fig. 6. Marine environment (tidal zone in La Rochelle). Tcc profiles measured (after drying) in RC structural elements by chemical analysis after various exposure times. x_c: *average carbonation depth after 10 years.*

in lab conditions (see previous sections) were observed *in situ*. This results from very weak drying, which can be considered here to be mainly the result of Darcian transport of liquid water with evaporation located at the exposed surface, given the weathering conditions and the type of materials (S_l remains very high in these RC structural elements, see [22]). In addition, microstructural surface alterations induced by carbonation or early-age drying are negligible in these RC structural elements (see also [22]).

6. Example of chloride ingress and service life predictions by means of the multi-species transport model (*level* 2) in tidal zone

All of the observed phenomena described in Section 5 cannot be predicted by the multi-species transport model developed in saturated conditions (*level* 2). Therefore in a lot of cases, a model that accounts at least for natural drying, and as far as possible for realistic wetting–drying cycles, cannot be avoided for a proper prediction of the service life of RC structures exposed to chlorides. However, it can be difficult to express the actual B.C. of structures *in situ* and to assess all the input data required by a sophisticated model such as *level* 4. Hence, it is worth investigating whether a simpler model as *level* 2 can be used for predictions even in tidal zone, in some cases. An example of SL prediction by means of the multi-species transport model (*level* 2) is presented in the present section. This example deals with the M120SF (RC) structural element in La Rochelle (see Section 5.3).

6.1. Tcc profile prediction

The level-2 model has been applied to predict the tcc profile of the M120SF structural element. The field tcc profile after 2-year exposure (see Fig. 6b) has been used to identify some of the input data of the model (the constant D_{Cl} and the *Freundlich's* parameters of the binding isotherm) by numerical inverse analysis. This indirect method (described in [34]) consists in analyzing the experimental data by using the model: a simple numerical algorithm is used to identify the D_{Cl} and *Freundlich's* parameters values, which best reproduce the experimental tcc profile (see Fig. 7a). This method is particularly appropriate to the monitoring of existing structures, since tcc profiles are the experimental data that are most often available and since no additional lab experiment is required. The porosity has been directly measured ($\phi = 0.074$). The initial chemical composition of the pore solution has been assessed by the analytical method described in [34]. Once these input data included in the model, it is then possible to predict the free or/and total chloride concentration profiles after longer exposure times, in view of prediction of future (long-term) evolution of the structural element. The tcc profiles after 4-, 10-, 50-, and 100-year exposure were thus predicted (see Fig. 7a).

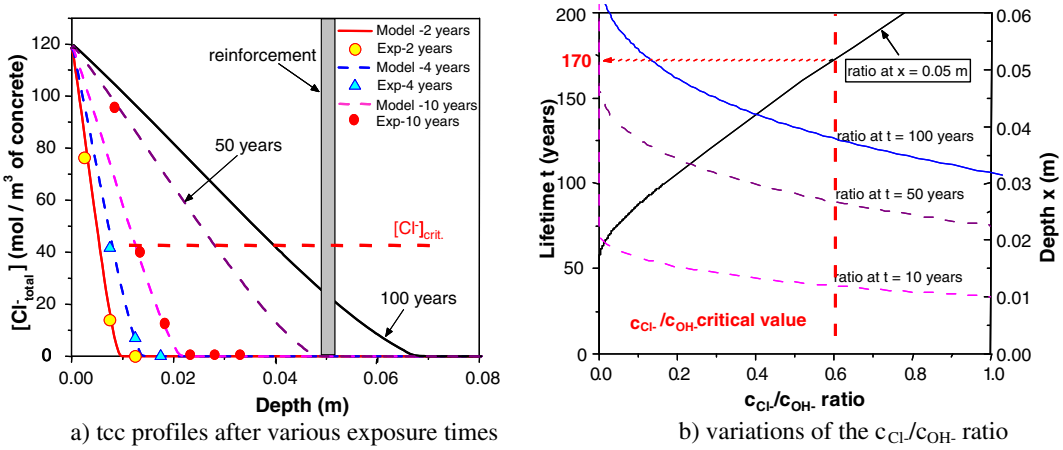

a) tcc profiles after various exposure times b) variations of the c_{Cl^-}/c_{OH^-} ratio

Fig. 7. M120SF (RC) structural element in marine environment (tidal zone in La Rochelle). Measurements and numerical simulations performed by the multi-species transport model (*level* 2).

Very good agreement with the available field tcc profiles at 4 and 10 years is observed, except within the surface zone where a significant higher tcc is measured (e.g. 139 and 215 mol/m^3 of concrete at depth x = 2.5 mm, for 4 and 10 years, respectively). This was expected from the analysis performed in Section 5.1. Therefore, beyond the advection zone, the same profile is measured as that predicted for the case of diffusion during the same period of time, since the degree of saturation allows diffusion of the chloride ions present in the pore solution towards the core, whatever the outer conditions [22]. Thus, the same observation is made *in situ* as in lab conditions (see Fig. 3d). This example highlights the validation of the level-2 model in field conditions (second stage of validation).

Hence, it seems that, for the cases where drying and drying–wetting cycles have a significant effect only within a restricted zone close to the surface (e.g. in the case of HPCs), and therefore where the assumption of sole diffusion is acceptable within the reminder zone of the structural element, a model developed in saturated conditions can be sufficient for SL prediction, since this is the front location which is critical for this purpose. This result is of importance from a practical point of view.

6.2. SL prediction

The front is often characterized by the so-called "critical" chloride concentration, assumed to be the concentration, which induces depassivation of the reinforcement surface and initiates iron dissolution. If the "critical" tcc is assumed to be 0.4% by unit mass of cement, as usually done [22,59], and if the level-2 model is assumed as valid for long-term predictions in the considered case, Fig. 7a shows that, according to the numerical simulations, the "critical" tcc will not be reached at the first layer of rebars (cover thickness = 50 mm) neither after 50 years nor after 100 years. The service life (when only the initiation period [27] is regarded) will therefore be higher.

It will be checked in the future, by comparison between experimental and numerical results after longer exposure times than 10 years, if *level* 2 is still valid. However, one should note that the approximation made when selecting the level of the model can be far smaller than that made when selecting the "critical" chloride concentration value, since the actual value may vary within a great extent, mainly as a result of the compositions of concrete and steel, of the characteristics of their interface, and of the environmental conditions [59,60].

The service life (within the initiation period) can be investigated in a more precise way by studying the evolution of the c_{Cl^-}/c_{OH^-} ratio (see Fig. 7b). Therefore, since the multi-species model allows the assessment of both the c_{Cl^-} and c_{OH^-} values, and assuming that depassivation occurs, and hence the end of the service life is reached, when the c_{Cl^-}/c_{OH^-} ratio is equal to 0.6 [5,61,62] at the first layer of rebars, it is possible to predict the SL based on this criterion. The numerical simulations provide a 170-year SL for this structural element (see Fig. 7b). This is in agreement with the performance-based specifications displayed in Table 1 and the values of the DIs measured on this HPC (ϕ = 0.074, $D_{app(mig)} = 0.04 \times 10^{-12}$ m^2 s^{-1}, $K_{app(gas)} = 43 \times 10^{-18}$ m^2 and $k_l = 10^{-5} \times 10^{-18}$ m^2): according to Table 1, in tidal zone, with such DI values, one should expect a service life higher than 120 years.

7. Concluding remarks

The approach proposed here, which is based on durability indicators and physically-based models, constitutes a useful and flexible tool for an efficient assessment and prediction of RC durability with regard to the protection against chloride-induced corrosion.

This approach offers greater freedom to engineers and designers. The achievement of specified levels of performance, for example based on the specifications proposed here, allows one to take advantage of all the technical, environmental and economical benefits of new concepts of mix-design and high-technology materials within the framework of sustainable development. An extended structural service life can be expected from these new trends, as confirmed by the field data already available. In addition, the multi-level concept allows one to apply the same methodology with simple tools for engineering purposes, as well as with advanced numerical models for accurate prediction in more complex cases.

More specifically, the multi-level model of chloride ingress proposed here can be used for:

- understanding of phenomena, e.g. to check assumptions and physical/chemical mechanisms associated with binding or coupled moisture-ion transport, as illustrated in this paper,
- assessment of input data by numerical analysis,
- concrete mix-design for a predefined durability of RC structures, by selecting the appropriate aluminate, C–S–H or SCM contents, in order to optimize the chemical effect (e.g. through the equations describing chloride binding) and the physical barrier (e.g. through chloride effective diffusion coefficient and liquid permeability),
- chloride ingress and SL predictions in various environmental conditions (at the design stage or for the monitoring of existing structures).

With regard to chloride binding, the simplified description (analytical formula, which includes physical adsorption and instantaneous *Friedel's* salt formation expressed as a function of the residual equivalent aluminate content) used with *level* 2, compared to *level* 3, is very convenient from a numerical point of view. It avoids the incorporation of the equations and of the additional ionic and solid species associated with the dissolution-precipitation reactions. The discontinuous feature of these equations can indeed induce numerical difficulties. In addition, the difference then obtained on the results can be quite acceptable in a lot of cases.

More generally, the numerical simulations reported in this paper show clearly that, on the one hand, *level* 2, which is an intermediate level of sophistication, is likely to provide quite sufficiently accurate predictions for a large number of practical cases. On the other hand, only the level-4 model, which combines liquid-water and water-vapour transport processes with aqueous electrolyte theory, is capable of reproducing all the effects of wetting–drying cycles, which often take place *in situ*, on the profiles and in particular on the (drastically affected) surface zone, and will allow long-term accurate predictions for every types of environment and material.

Acknowledgements

The authors would like to thank the members of the AFGC working group "Durability indicators", as well as the LRPCs of Bordeaux, Clermont-Ferrand, Est Parisien, Lille, Lyon, and Saint-Brieuc (France), who took part to the "BHP 2000" and LPC Projects.

References

[1] Baroghel-Bouny V, Andrade C, Torrent R, Scrivener K, Baroghel-Bouny V, Andrade C, Torrent R, Scrivener K, editors. Proceedings of international RILEM workshop on performance based evaluation and indicators for concrete durability, March 19–21, 2006, Madrid, Spain. RILEM Publ.: Bagneux; 2007 [PRO 47].

[2] Ishida T, Mabrouk RTS, Maekawa K. An integrated computational framework for performance evaluation of cementitious materials and structures under various environmental actions. In: Ulm FJ, Bazant ZP, Wittmann FH, editors. Proceedings of the sixth international conference "creep, shrinkage and durability mechanics of concrete and other quasi-brittle materials concreep'6", August 20–22, 2001, Cambridge, USA: Elsevier; 2001. p. 511–6.
[3] Maekawa K, Ishida T, Chijiwa N. Computational life-cycle assessment of structural concrete subjected to coupled severe environment and mechanistic actions. In: Toutlemonde F, Sakai K, Gjørv OE, Banthia N, editors. Proceedings of the fifth international conference on concrete under severe conditions: environment and loading (CONSEC'07), June 4–6, 2007, Tours, France, vol. 1. Paris: LCPC; 2007. p. 3–18.
[4] Baroghel-Bouny V. Durability indicators: relevant tools for an improved assessment of RC durability. In: Toutlemonde F, Sakai K, Gjørv OE, Banthia N, editors. Proceedings of fifth international conference on concrete under severe conditions: environment and loading (CONSEC'07), June 4–6, 2007, vol. 1. Tours, France: LCPC; 2007. p. 67–84.
[5] Baroghel-Bouny V et al. Concrete design for a given structure service life – durability management with regards to reinforcement corrosion and alkali–silica reaction. State-of-the-art and guide for the implementation of a predictive performance approach based upon durability indicators. Scientific and technical documents of AFGC (AFGC, Paris, issue in French: 2004 and issue in English: 2007). 240 p.
[6] Kirkpatrick TJ, Weyers RE, Sprinkel MM, Anderson-Cook CM. Impact of specification changes on chloride-induced corrosion service life of bridge decks. Cem Concr Res 2002;32(8):1189–97.
[7] FIB 2006. Model code for service life design. FIB Bull 2006;34:110.
[8] Thiery M, Cremona C, Baroghel-Bouny V. Application of the reliability theory to the assessment of the corrosion risk due to carbonation. In: Türkeri AN, Sengül Ö, editors. Proceedings of 11th international conference on durability of building materials and components (11DBMC), May 11–14, 2008, Istanbul, Turkey, vol. 4; 2008. p. 1551–60.
[9] Yeomans SR. Performance of black, galvanized, and epoxy-coated reinforcing steels in chloride – contaminated concrete. Corrosion 1994;50(1):72–81.
[10] Francy O. Modelling of chloride ions ingress in partially water saturated mortars. PhD thesis, Paul Sabatier Univ., Toulouse, France; 1998, 171 p [in French].
[11] Nguyen TQ. Physicochemical modelling of chloride ions ingress in cementitious materials (in French). PhD thesis, ENPC, Marne-la-Vallée, France; 2007. 233 p.
[12] Saetta AV, Scotta RV, Vitaliani RV. Analysis of chloride diffusion into partially saturated concrete. ACI Mater J 1993;90(5):441–51.
[13] Marchand J, Samson E, Maltais Y, Lee RJ, Sahu S. Predicting the performance of concrete structures exposed to chemically aggressive environment – field validation. Mater Struct 2002;35:623–31.
[14] Johannesson BF. A theoretical model describing diffusion of a mixture of different types of ions in pore solution of concrete coupled to moisture transport. Cem Concr Res 2003;33:481–8.
[15] Meijers SJH, Bijen JMJM, de Borst R, Fraaij ALA. Computational results of a model for chloride ingress in concrete including convection, drying–wetting cycles and carbonation. Mater Struct 2005;38:145–54.
[16] Nilsson LO. A model for convection of chloride. In: Frederiksen V, editor. A system for estimation of chloride ingress into concrete. Theoretical background, HETEK report no. 83. The Danish Road Directorate, Copenhagen; 1997. p. 47–68 [chapter 7].
[17] Swaddiwudhipong S, Wong SF, Wee TH, Lee SL. Chloride ingress in partially and fully saturated concretes. Con Sci Eng 2000;2:17–31.
[18] Nilsson LO. WP4 report – modelling of chloride ingress. CHLORTEST – EU funded research project "resistance of concrete to chloride ingress – from laboratory tests to in-field performance" G6RD-CT-2002-0085. Deliverables D14-15; 2005, 112 p.
[19] Recommended methods for the measurement of durability-related properties. In: Proceedings of journal technology AFPC-AFREM 'Durabilité des Bétons', December 11–12, 1997. Toulouse, France, Toulouse: LMDC; 1998 [in French].
[20] Baroghel-Bouny V, Belin P, Castellote M, Rafa N, Rougeau P., Yssorche-Cubaynes MP. Which toolkit for durability evaluation as regards chloride ingress into concrete? Part I: comparison between various methods for assessing the chloride diffusion coefficient of concrete in saturated conditions. In: Andrade C, Kropp J, editors. Proceedings of third international RILEM workshop "testing and modelling chloride ingress into concrete", September 9–10, 2002, Madrid, Spain, Bagneux, RILEM Publ.; 2004. p. 105–36 [PRO 38].
[21] Tang L. Guideline for practical use of methods for testing the resistance of concrete to chloride ingress, CHLORTEST – EU funded research project "Resistance of concrete to chloride ingress – from laboratory tests to in-field performance" G6RD-CT-2002-0085. Deliverable D23; 2005. 14 p.
[22] Baroghel-Bouny V, Gawsewitch J, Belin P, Ounoughi K, Arnaud S, Olivier G, et al. Ageing of concretes in natural environments: an experiment for the 21st century. IV – results on cores extracted from field-exposed test specimens of various sites at the first times of measurement. Bul Lab Ponts Chaus 2004;249:49–100.
[23] Alexander MG, Mackechnie JR. Predictions of long-term chloride ingress from marine exposure trials. In: Hooton RD, Thomas MDA, Marchand J, Beaudoin JJ, editors. Materials science of concrete. Skalny JP, editors. Ion and mass transport in cement-based materials, Special vol.. American Ceramic Society; 2001. p. 281–91.
[24] Kakizaki M, Edahiro H, Fujii K, Nakase H. Effects of mixture proportions on permeability and pore structure of high-fluidity concretes. In: Malhotra VM, editor. Proceedings of fifth CANMET/ACI international conference on durability of concrete, June 4–9, 2000, SP-192, vol. II. Barcelona, Spain: ACI; 2000. p. 755–72.
[25] Du Preez AA, Alexander MG. A site study of durability indexes for concrete in marine conditions. Mater Struct 2004;37(267):146–54.
[26] Lu X. Application of the Nernst–Einstein equation to concrete. Cem Concr Res 1997;27(2):293–302.
[27] Tuutti K., Corrosion of steel in concrete. Report 4.82. Stockholm, Sweden, Swedish Cem. Conc. Res. Inst. (CBI); 1982.
[28] Eymard R, Gallouet T, Herbin R. The finite volume method. In: Ciarlet P, Lions JL, editors. Handbook of numerical analysis; 2000.
[29] Nguyen TQ, Baroghel-Bouny V, Dangla P, Belin P, Multi-level modelling of chloride ingress into saturated concrete. In: Baroghel-Bouny V, Andrade C, Torrent R, Scrivener K, editors. Proceedings of international RILEM workshop on performance based evaluation and indicators for concrete durability, March 19–21, 2006, Madrid, Spain. Bagneux: RILEM Publ.; 2007. p. 145–55 [PRO 47].
[30] Bigas JP, Chloride ions diffusion in mortars (in French). PhD thesis, INSA Toulouse, France; 1994. 201 p.
[31] Achari G, Chatterji S, Joshi RC. Evidence of the concentration dependent ionic diffusivity though saturated porous media. In: Nilsson LO, Ollivier JP, editors. Proceedings of first international RILEM workshop "chloride penetration into concrete", October 15–18, 1995, St-Rémy-lès-Chevreuse, France. Cachan: RILEM; 1997. p. 74–6.
[32] Tang L. Concentration dependence of diffusion and migration of chloride ions. Cem Concr Res 1999;29:1469–74.
[33] Truc O, Ollivier JP, Nilsson LO. Multi-species transport in saturated cement-based materials. In: Andrade C, Kropp J, editors. Proceedings of the second international RILEM workshop "testing and modelling chloride ingress into concrete", September 11–12, 2000, Paris, France. Paris: RILEM; 2000. p. 247–59.
[34] Nguyen TQ, Baroghel-Bouny V, Dangla P. Prediction of chloride ingress into saturated concrete on the basis of a multi-species model by numerical calculations. Comp Conc 2006;3(6):401–22.
[35] Andrade C. Calculation of chloride diffusion coefficients in concrete from ionic migration measurements. Cem Concr Res 1993;23(3):724–42.
[36] Masi M, Colella D, Radaelli G, Bertolini L. Simulation of chloride penetration in cement-based materials. Cem Concr Res 1997;27(10):1591–601.
[37] Samson E, Marchand J. Numerical solution of the extended Nernst–Planck model. J Colloid Interf Sci 1999;215:1–8.
[38] Baroghel-Bouny V, Nguyen TQ, Dangla P, Belin P. Assessment of chloride binding isotherms. In: Schlangen E, de Schutter G, editor. Proceedings of the international symposium on concrete modelling (CONMOD'08), May 26–28, 2008, Delft, The Netherlands. Bagneux: RILEM Publ.; 2008. p. 733–s43 [PRO 58].
[39] Tang L, Nilsson LO. Chloride binding capacity and binding isotherms of OPC pastes and mortars. Cem Concr Res 1993;23:247–53.
[40] Beaudoin JJ, Ramachandran VS, Feldman RF. Interaction of chloride and C–S–H. Cem Concr Res 1999;20:875–83.
[41] Suryavanshi AK, Scantlebury JD, Lyon SB. Mechanism of Friedel's salt formation in cements rich in tri-calcium aluminate. Cem Concr Res 1996;26:717–27.
[42] Birnin-Yauri UA, Glasser FP. Friedel's salt, Ca_2 $Al(OH)_6$ (Cl, OH)$2H_2O$: Its solid solutions and their role in chloride binding. Cem Concr Res 1998;28:1713–23.
[43] Helfferich F. Ion exchange. New York: McGraw-Hill; 1962.
[44] Newman JS. Electrochemical systems. 2nd ed. Englewood Cliffs: Prentice Hall; 1991.
[45] Mounanga P, Khelidj A, Loukili A, Baroghel-Bouny V. Predicting $Ca(OH)_2$ content and chemical shrinkage of hydrating cement pastes using analytical approach. Cem Concr Res 2004;34(2):255–65.
[46] Nguyen TQ, Dangla P, Baroghel-Bouny V, Petit L. An approach for the physicochemical modelling of chloride ingress into cementitious materials. In: Proceedings 12th international congress on the chemistry of cement (ICCC 2007), July 8–13, Montréal, Québec, Canada; 2007.
[47] Bentz DP, Garboczi EJ, Lagergren ES. Multi-scale microstructural modelling of concrete diffusivity: identification of significant variables. Cem Concr Aggr 1998;20:129–39.
[48] Baroghel-Bouny V, Mainguy M, Coussy O. Isothermal drying process in weakly permeable cementitious materials – assessment of water permeability. In: Hooton RD, Thomas MDA, Marchand J, Beaudoin JJ, editors. Materials science of concrete. Skalny JP, editors. Ion and mass transport in cement-based materials, Special vol.. Westerville: American Ceramic Society; 2001. p. 59–80.
[49] Baroghel-Bouny V. Water vapour sorption experiments on hardened cementitious materials. Part II: essential tool for assessment of transport properties and for durability prediction. Cem Concr Res 2007;37(3):438–54.
[50] Thiery M, Baroghel-Bouny V, Bourneton N, Villain G, Stefani C. Modelling of drying of concrete – analysis of the different moisture transport modes (in French). Rev Euro Gén Civ 2007;11(5):541–77.
[51] Lin CL, Lee LS. A two-ionic-parameter approach for ion activity coefficients of aqueous electrolyte solutions. Fluid Phase Equilibria 2003;205:69–88.
[52] Nguyen TQ, Baroghel-Bouny V, Dangla P. A physical model for estimating the coupled transport of moisture and chlorides in concrete. In: Toutlemonde F, Sakai K, Gjørv OE, Banthia N, editors. Proceedings of the fifth international conference on concrete under severe conditions: environment and loading (CONSEC'07), June 4–6, 2007, Tours, France. Paris: LCPC, vol. 1; 2007. p. 331–42.

[53] Baroghel-Bouny V. Water vapour sorption experiments on hardened cementitious materials. Part I: essential tool for analysis of hygral behaviour and its relation to pore structure. Cem Concr Res 2007;37(3):414–37.
[54] Buchwald A. Determination of the ion diffusion coefficient in moisture and salt loaded masonry materials by impedance spectroscopy. In: Proceedings of the third international PhD symposium, October 11–13, Vienna, Austria, vol. 2; 2000. p. 475–82.
[55] Chaussadent T, Arliguie G. AFREM test procedures concerning chlorides in concrete: extraction and titration methods. Mater Struct 1999;32(217):230–4.
[56] Analysis of water soluble chloride content in concrete, RILEM TC 178-TMC Recommendation. Mater Struct 2002; 35(253): 586–8.
[57] Otsuki N, Nagataki S, Nakashita K. Evaluation of $AgNO_3$ solution spray method for measurement of chloride penetration into hardened cementitious matrix materials. ACI Mater J 1992;89(6):587–92.
[58] Hong K, Hooton RD. Effects of cyclic chloride exposure on penetration of concrete cover. Cem Concr Res 1999;29:1379–86.
[59] Glass GK, Buenfeld NR. Chloride threshold levels for corrosion induced deterioration of steel in concrete. In: Nilsson LO, Ollivier JP, editors. Proceedings of thefirst International RILEM workshop ‘‘chloride penetration into concrete”, October 15–18, 1995, Saint-Rémy-lès-Chevreuse, France. Cachan:RILEM; 1997. p. 429–40.
[60] Alonso C, Andrade C, Castellote M, Castro P. Chloride threshold values to depassivate reinforcing bars embedded in a standardized OPC mortar. Cem Conc Res 2000;30(7):1047–55.
[61] Hausmann DA. Steel corrosion in concrete: how does it occur? Mater Prot 1967;4(11):19–23.
[62] Gouda VK. Corrosion and corrosion inhibition of reinforcing steel. Br Corros J 1970;5:198–203.